EPJ Web of Conferences **20**, 02002 (2012)
DOI: 10.1051/epjconf/20122002002

η production off the proton in a chiral quark approach

Jun He

[1] Research Center for Hadron and CSR Physics, Institute of Modern Physics of CAS & Lanzhou University
[2] Nuclear theory group, Institute of Modern Physics, Chinese Academy of Sciences

Abstract. we report our chiral quark approach for the eta productions combined with the potential model. Starting from an effective chiral Lagrangian, the amplitude of pseudoscalar production is derived and connected to the helicity and decay amplitudes under the $SU(3)$ symmetry. The breaking of the $SU(3)$ symmetry is introduced by the configuraton mixing which can be calculated from the potential model. To extend our model to higher energy region where CLAS and CBELSA/TAPS Collaborations release their new data recently, Reggeized trajectories instead of simple ρ and ω poles is adopted. Both the spectrum and the η productions are calculated and well compared with the experiment data. The results suggest that the contribution from "missing" resonances, with masses below 2 GeV, is found to be negligible in the considered processes.

1 Introduction

After the discovery of the first resonance of nucleon Δ in the πN scattering, more and more resonances are found in the experiment. Due to the difficulty of solving the QCD in the non-perturbative region, the internal structure of nucleon and its resonances is still unclear and many experiment and theoretical efforts are paid in this area. The main information about nucleon resonances in the early days is from πN scattering, and it is still the main source of the data which is used to explore the nucleon resonances as shown by the Particle Data Group (PDG). The photoproduction become more popular due to the cleanness of the electromagnetic probe.

In both πN scattering and photoproduction the resonances should be studied through the meson production. The most nucleon resonances are observed in the π production process. However the puzzles in the spectrum, such as "missing resonances", encourage people to study other channels. The η production is appropriate to study the properties of the nucleon resonances (N^*). In the π production processes, an serious problem is that both Δ with three half isospin and nucleon with half isospin and their resonances are involved. As listed in the PDG, there exist twenty five state in the energy below 2 GeV, which make the analysis very difficult considered the large Breit-Wigner width of the resonances. However in η production, the zero isospin of η will filter out all the Δ resonances. The number of resonances with the energy below 2 GeV in the η production is twelve, only about half as much as in the number in the π productions.

Among some twenty N^*s, the importance of the lightest S_{11} resonance, $N(1535)$ to understand internal structure of nucleon resonances, such as the mixing angles have been suggested by many authors [1–8] and the possible multiquark components have proposed [9, 10]. The η productions off proton is dominant by the contribution from $S_{11}(1535)$. Hence the η productions is important to explore the internal structure of $S_{11}(1535)$.

Due to the importance of the η producitons, it has been studied by hadronic and electromagnetic probes, essentially off the nucleon. The data for $\pi N \to \eta N$ come mainly from measurements performed in 70s [11–14] and suffer from some inconsistencies [15], except a recent experiment performed at BNL, using the Crystal Ball spectrometer [16, 17]. The published CB data [17] are high quality mea-

surements, though limited to the close to threshold kinematics. For the photoproduction process, a healthy amount of data has been published in recent years for both differential cross section [18–21] and polarized beam asymmetry [21, 22]. Recently CBELSA/TAPS [23] and CLAS [24] Collaborations released new data with higher precision and higher energies [24].

The large amount of the data have attracted much theoretical interest and many groups are working on analysis of the experiment data, such as,the SAID group, MAID group, EBAC dynamical coupled-channels model (EBAC-DCC) and many other authors [25–35]. All those works are starting from effective Lagrangian approaches with meson-baryon degrees of freedom. So the interanl structure of the nucleon resoance should be invetstigated after its properties, such as mass decay width, helicity amplitudes, have been extracted from the above analysis.

Our approach based on subnucleonic degrees of freedom, via chiral constituent quark models (χCQM) have been developed and successfully applied to the interpretation of photoproduction of pseudoscalar mesons on the proton, namely, $\gamma p \to \pi N$ [36], ηp [37,38,3], $K^+\Lambda$ [33], as well as the process $\pi^- p \to \eta n$ [39]. This chiral quark approach is starting from the chiral effective Lagrangian and applying a second quantization under the $SU(3)$ symmetry. The breaking of $SU(3)$ symmetry is introduced by an free parameters for each parameters. And the study is limited in the low energy region due to the complication in the higher energy region. Here we report the recent progress to include the $SU(3)$ symmetry breaking though potential model and to extend the energy region to the higher energy region [40].

The report is organized as follows. In Section 2, the theoretical frame of our χCQM approach are presented especially the connection of the total amplitudes and the helicity and decay amplitudes, and the Reggeized model are briefly presented. The fitting procedure and numerical results are reported in section 3. The report ends with a brief summary.

2 Theoretical Frame

In this section we will recall the chiral quark model we used and connect the *CGLN* amplitudes for the meson productions to the helicity amplitudes and decay amplitudes of the nucleon resonances. The potential models are introduced to describe the $SU(3)$ symmetry breaking.

2.1 Chiral effective Lagrangian

Chiral quark model approaches, are based on the low energy chiral effective Lagrangian [41,42]

$$\mathcal{L} = \bar{\psi}[\gamma_\mu(i\partial^\mu + V^\mu + \gamma_5 A^\mu) - m]\psi + \cdots, \tag{1}$$

where vector (V^μ) and axial (A^μ) currents read,

$$V^\mu = \frac{1}{2}(\xi\partial^\mu\xi^\dagger + \xi^\dagger\partial^\mu\xi)\ ,\ A^\mu = \frac{1}{2i}(\xi\partial^\mu\xi^\dagger - \xi^\dagger\partial^\mu\xi), \tag{2}$$

with $\xi = \exp(i\phi_m/f_m)$ and f_m the meson decay constant. ψ and ϕ_m are the quark and meson fields, respectively.

There are four components for the productions of pseudoscalar mesons based on the QCD Lagrangian,

$$\mathcal{M}_{fi} = \langle N_f|H_{m,e}|N_i\rangle + \sum_j \left\{ \frac{\langle N_f|H_m|N_j\rangle\langle N_j|H_e|N_i\rangle}{E_i + \omega - E_j} + \frac{\langle N_f|H_e|N_j\rangle\langle N_j|H_m|N_i\rangle}{E_i - \omega_m - E_j} \right\} + \mathcal{M}_T \tag{3}$$

where $N_i(N_f)$ is the initial (final) state of the nucleon, and $\omega(\omega_m)$ represents the energy of incoming (outgoing) photons (mesons). The first term in Eq. (3) is a seagull term. It is generated by the gauge transformation of the axial vector A_μ in the QCD Lagrangian. This term, being proportional to the electric charge of the outgoing mesons, does not contribute to the production of the neutral meson, such as η-meson. The second and third terms correspond to the s- and u-channels, respectively. The last term is the t-channel contribution.

2.2 Nucleon resonance contributions

The nucleon resonances is important in the s and u-channels. For the u-channel, its contributions are less sensitive to the detail structure of resonance than those in the s-channel. So it is reasonable to treat the higher n contributions as degenerate.

For s-channel, in general one can write the amplitudes as

$$\mathcal{M}_R = \frac{2M_R}{s - M_R^2 - iM_R\Gamma(\mathbf{q})} e^{-\frac{\mathbf{k}^2+\mathbf{q}^2}{6\alpha^2}} O_R, \tag{4}$$

where $\sqrt{s} = E_N + \omega_\gamma = E_S + \omega_m$ is the total energy of the system, and O_R is determined by the structure of each resonance. $\Gamma(\mathbf{q})$ in Eq. (4) is the total width of the resonance, and a function of the final state momentum $\mathbf{q}$.

The operator for resonance has a general structure,

$$O_R = g_R A[f_1^R \boldsymbol{\sigma}\cdot\boldsymbol{\epsilon} + if_2^R \boldsymbol{\sigma}\cdot\hat{\mathbf{q}}\boldsymbol{\sigma}\cdot(\hat{\mathbf{k}}\times\boldsymbol{\epsilon}) + f_3^R \boldsymbol{\sigma}\cdot\hat{\mathbf{k}}\hat{\mathbf{q}}\cdot\boldsymbol{\epsilon} + f_4^R \boldsymbol{\sigma}\cdot\hat{\mathbf{q}}\boldsymbol{\epsilon}\cdot\hat{\mathbf{q}}] \tag{5}$$

for the pseudoscalar meson photoproductions, where g_R is an isospin factor, A is the meson decay amplitude, and f^R is the phototransition amplitude [42]. With the g_R we can separate the contribution from multiplets under the $SU(3)$ symmetry as

$$\begin{aligned}
O_{[56,^2N]} &= -O_{\gamma p\to\eta p} + 2O_{\gamma p\to K^+\Lambda} \\
O_{[70,^2N]} &= +O_{\gamma p\to\eta p} - O_{\gamma p\to K^+\Lambda} \\
O_{[56,^2N]} - O_{[70,^4N]} &= -O_{\gamma n\to\eta n} + 2O_{\gamma n\to K^0\Lambda} \\
-\frac{8}{3}O_{[56,^4\Delta]} - O_{[70,^2\Delta]} &= O_{\gamma n\to K^0\Sigma^0} + 2O_{\gamma n\to\eta n} - 3O_{\gamma n\to K^0\Lambda}
\end{aligned} \tag{6}$$

where the operators, such as $O_{\gamma p\to\eta p}$ and $O_{[56,^2N]}$ are the operators for the corresponding processes and multiplet.

The operators O_n for an processes for n-shell in the harmonic oscillator basis can be calculated by the second-quantization and found explicitly in [42]. Obviously for $O_{[56,^2N]}$, $O_{[70,^2N]}$ and $O_{[70,^2N]}$, we can obtain the contribution from each multiplet directly for the process without Δ resonances contribution, such as $\gamma p \to \eta p$. However for the process with Δ resonances, the contribution from two Δ multiplet should be separated. It is usually easy to calculate in quark model because they are state with the same total angular moment and orbital angular moment and we only need the ratio.

Now we can separate the contribution for the partial wave l of the two multiplets to any n. Then using the standard multipole expansion of CGLN amplitudes,

$$\begin{aligned}
f_1 &= \sum_{\ell=0}^{\infty}[\ell M_{\ell+} + E_{\ell+}]P'_{\ell+1} + [(\ell+1)M_{\ell-} + E_{\ell-}]P'_{\ell-1} \\
f_2 &= \sum_{\ell=1}^{\infty}[(\ell+1)M_{\ell+} + \ell M_{\ell-}]P'_{\ell} \\
f_3 &= \sum_{\ell=1}^{\infty}[-M_{\ell+} + E_{\ell+}]P''_{\ell+1} + [M_{\ell-} + E_{\ell-}]P''_{\ell-1} \\
f_4 &= \sum_{\ell=2}^{\infty}[M_{\ell+} - E_{\ell+} - M_{\ell-} - E_{\ell-}]P''_{\ell}
\end{aligned} \tag{7}$$

where the P_l are the Legendre function.

After separation the total operator to the explicit multiplet the results by multipole expansion can be connected to the CGLN amplitudes for each resonance in the Table III in Ref. [42]. Our calculation is up to $N = 4$ and both proton and neutron. Only the results for the proton resonances with $N = 1, 2$ are presented in Tables 1. We can find results here for the $N = 1, 2$ case is same as theirs(with some typo corrected).

Table 1. CGLN amplitudes for proton target.

state		f_1	f_2	f_3	f_4
$\Delta(^4S_s)\,\frac{3}{2}$	P_{33}	$\frac{3kx}{2m_q}$	$\frac{k}{m_q}$	$-\frac{3k}{2m_q}$	0
$N(^2P_M)\,\frac{1}{2}$	S_{11}	$\frac{k(k+2m_q)}{24\alpha m_q}$	0	0	0
$N(^2P_M)\,\frac{3}{2}$	D_{13}	$-\frac{k(k+2m_q)}{36\alpha m_q}$	$-\frac{k^2x}{12\alpha m_q}$	0	$\frac{k}{6\alpha}$
$\Delta(^2P_M)\,\frac{1}{2}$	S_{31}	$-\frac{k(k-6m_q)}{36\alpha m_q}$	0	0	0
$\Delta(^2P_M)\,\frac{3}{2}$	D_{33}	$\frac{k(k-6m_q)}{54\alpha m_q}$	$\frac{k^2x}{18\alpha m_q}$	0	$\frac{k}{3\alpha}$
$N(^2S_s)\,\frac{1}{2}$	P_{11}	0	$-\frac{k^3}{216\alpha^2 m_q}$	0	0
$\Delta(^4S_s)\,\frac{3}{2}$	P_{33}	$\frac{k^3x}{72\alpha^2 m_q}$	$\frac{k^3}{108\alpha^2 m_q}$	$-\frac{k^3}{72\alpha^2 m_q}$	0
$N(^2D_s)\,\frac{3}{2}$	P_{13}	$\frac{k^2(k+2m_q)x}{72\alpha^2 m_q}$	$\frac{k^3}{216\alpha^2 m_q}$	$\frac{k^2}{36\alpha^2}$	0
$N(^2D_s)\,\frac{5}{2}$	F_{15}	$-\frac{k^2(k+2m_q)x}{180\alpha^2 m_q}$	$\frac{k^3(1-5x^2)}{360\alpha^2 m_q}$	$-\frac{k^2}{90\alpha^2}$	$\frac{k^2x}{18\alpha^2}$
$\Delta(^4D_s)\,\frac{1}{2}$	P_{31}	0	$-\frac{k^3}{216\alpha^2 m_q}$	0	0
$\Delta(^4D_s)\,\frac{3}{2}$	P_{33}	0	$-\frac{k^3}{216\alpha^2 m_q}$	$\frac{k^3}{72\alpha^2 m_q}$	0
$\Delta(^4D_s)\,\frac{5}{2}$	F_{35}	$\frac{k^3x}{252\alpha^2 m_q}$	$\frac{k^3(5x^2-1)}{1260\alpha^2 m_q}$	$\frac{k^3}{420\alpha^2 m_q}$	$-\frac{k^3x}{84\alpha^2 m_q}$
$\Delta(^4D_s)\,\frac{7}{2}$	F_{37}	$\frac{k^3x(7x^2-3)}{168\alpha^2 m_q}$	$\frac{k^3(5x^2-1)}{210\alpha^2 m_q}$	$\frac{k^3(1-7x^2)}{168\alpha^2 m_q}$	$\frac{k^3x}{84\alpha^2 m_q}$
$N(^2S_M)\,\frac{1}{2}$	P_{11}	0	$-\frac{k^3}{432\alpha^2 m_q}$	0	0
$\Delta(^2S_M)\,\frac{1}{2}$	P_{31}	0	$\frac{k^3}{648\alpha^2 m_q}$	0	0
$N(^2D_M)\,\frac{3}{2}$	P_{13}	$\frac{k^2(k+2m_q)x}{144\alpha^2 m_q}$	$\frac{k^3}{432\alpha^2 m_q}$	$\frac{k^2}{72\alpha^2}$	0
$N(^2D_M)\,\frac{5}{2}$	F_{15}	$-\frac{k^2(k+2m_q)x}{360\alpha^2 m_q}$	$\frac{k^3(1-5x^2)}{720\alpha^2 m_q}$	$-\frac{k^2}{180\alpha^2}$	$\frac{k^2x}{36\alpha^2}$
$\Delta(^2D_M)\,\frac{3}{2}$	P_{33}	$-\frac{k^2(k-6m_q)x}{216\alpha^2 m_q}$	$-\frac{k^3}{648\alpha^2 m_q}$	$\frac{k^2}{36\alpha^2}$	0
$\Delta(^2D_M)\,\frac{5}{2}$	F_{35}	$\frac{k^2(k-6m_q)x}{540\alpha^2 m_q}$	$\frac{k^3(5x^2-1)}{1080\alpha^2 m_q}$	$-\frac{k^2}{90\alpha^2}$	$\frac{k^2x}{18\alpha^2}$

2.3 Relation to helicity amplitudes and decay width

Usually experimental amplitudes (T-matrix) are presented in the helicity basis, which are given as matrices in the space spanned by the initial and final helicity states [43],

$$A_{\mu\lambda}(\theta,\phi) = \sum_j (2j+1)\, A^j_{\mu\lambda}\, d^j_{\lambda\mu}(\theta)\, e^{i(\lambda-\mu)\phi} \ . \tag{8}$$

where θ is the c.m. scattering angles between photon and outgoing meson. Here $\lambda = \lambda_\gamma - \lambda_i$ and $\mu = \lambda_m - \lambda_f = -\lambda_f$ are the initial and final state helicities with λ_γ, λ_i, λ_m and λ_f being the helicity of the photon, of the initial nucleon, of the meson and of the final nucleon, respectively. The helicity elements $A^j_{\mu\lambda}$ in its form, however, do not have a definite parity. Parity eigenstates are projected out by the following linear combinations [43,44]

$$C^{l+}_\lambda = \frac{1}{\sqrt{2}}\left(A^j_{1/2\,\lambda} + A^j_{-1/2\,\lambda}\right) \ , \tag{9}$$

$$C^{(l+1)-}_\lambda = \frac{1}{\sqrt{2}}\left(A^j_{1/2\,\lambda} - A^j_{-1/2\,\lambda}\right) \ , \tag{10}$$

where $l\pm$ is the orbital angular momentum of the meson in the final state and total angular moment $j = l \pm 1/2$.

We are interested in the intermediate resonances, the $C_\lambda^{l\pm}$ can be written as Breit-Wigner form with background as,

$$C_\lambda^{l\pm}(W) = -\sum_{N^*} \epsilon \left(\frac{\Gamma_\gamma^\lambda \Gamma_\pi}{kq}\right)^{1/2} \frac{M}{W^2 - M^{*2} - iM\Gamma} + \text{background} \tag{11}$$

where Γ is the total decay width of the resonance N^* , Γ_γ^λ and Γ_π are the partial width for gamma (with the helicity λ) and pion emission. k and q are the momentum carried by the photon and the pion, respectively. The relative sign of each term is included in the parameter $\epsilon = \pm 1$. We can introduce the helicity amplitudes for the electromagnetic couplings as

$$C_\lambda^{l\pm} = \left(\frac{1}{(2j+1)\pi} \frac{k}{q} \frac{M_N}{M_R} \frac{\Gamma_\pi}{\Gamma^2}\right)^{1/2} A_\lambda^{j^P} \tag{12}$$

Theoretically, the amplitude $C_\lambda^{l\pm}(M^*)$ may be computed as[45]

$$C(W) = i \langle N|H_\pi|N^*\rangle \frac{M}{W^2 - M_R^2 - iM\Gamma} \langle N^*|H_\gamma|N\rangle \tag{13}$$

So, the electromagnetic helicity amplitudes $A_{1/2}^N$, $A_{3/2}^N$ and $S_{1/2}^N$ introduced in that way are related to the matrix elements of the electromagnetic interaction Hamiltonian according to

$$A_\lambda = \sqrt{\frac{2\pi\alpha}{|\boldsymbol{k}|}} \langle X; J\lambda|H_{em}|N; \frac{1}{2}\lambda - 1\rangle \tag{14}$$

$$A_\nu = \langle X; J\nu|H_m|N; \frac{1}{2}\nu\rangle \tag{15}$$

If we know the wave functions, it is easy to obtain helicity and strong decay amplitudes by the Hamiltonian. Here from the wave functions which have the definite symmetry [46], we obtain the wave functions used up to $N = 4$. With them, we presented the results of amplitudes in Table 2.

Then one can then write the Hebb-Walker amplitudes from A_λ as [47],

$$A_{l\pm} = \mp C_{\pi N}^I f A_{1/2} \tag{16}$$

$$B_{l\pm} = \pm C_{\pi N}^I f \sqrt{\frac{4}{l(l+2)}} A_{3/2} \tag{17}$$

$$C_{l\pm} = \mp C_{\pi N}^I f \frac{Q}{|\boldsymbol{k}_C|} S_{1/2}^N \tag{18}$$

$$\tag{19}$$

Where

$$f = [\frac{m_N E_N}{M_R^2} \frac{1}{(2J+1)\pi} |\boldsymbol{k}|]^{1/2} \frac{M_R}{s - M_R^2 + iM_R\Gamma(\boldsymbol{q})} A^m \tag{20}$$

where $C_{\pi N}^I$ represents the Clebsch-Gordan coefficient relted to the isospin coupling in the outgoing channel, and $\Gamma_l^m = \frac{|\boldsymbol{q}|E_N}{M_R} |A^m/C_{\pi N}^I|^2$.

With the helicity amplitudes of photon transition and meson decay we can obtain the CGLN amplitudes of each resonances also. We find the results is same as those obtained by the method in the previous subsection 3 for both proton and neutron resonances up to $N = 4$ shell Here the results for proton resonances with $N = 1, 2$ are presented in Tables 1 Hence the total amplitudes by the second quantization and separation procedure is equivalent to the one calculated from the helicity and strong decay amplitudes under the $SU(6)$ symmetry.

For the π induced meson productions, the similar results also can be found.

Table 2. Helicity amplitudes and partial wave meson decay amplitudes. For the decay amplitudes, the common factors can be found in Ref. [42].

	$A^p_{3/2}$	$A^p_{1/2}$	A^m_l
$\Delta(^4S_s)\,\frac{3}{2}$	$-\frac{2k}{\sqrt{3}m_q}$	$-\frac{2k}{3m_q}$	$\frac{3}{2}$
$N(^2P_M)\,\frac{3}{2}$	$\frac{i\sqrt{\frac{2}{3}}k}{\alpha}$	$-\frac{i\sqrt{2}k(k-m_q)}{3\alpha m_q}$	$-\frac{i}{3\sqrt{2}}$
$N(^2P_M)\,\frac{1}{2}$	0	$\frac{ik(k+2m_q)}{3\alpha m_q}$	$-\frac{i}{2\sqrt{2}}$
$\Delta(^2P_M)\,\frac{3}{2}$	$-\frac{i\sqrt{\frac{2}{3}}k}{\alpha}$	$-\frac{i\sqrt{2}k(k+3m_q)}{9\alpha m_q}$	$\frac{i\sqrt{2}}{3}$
$\Delta(^2P_M)\,\frac{1}{2}$	0	$\frac{ik(k-6m_q)}{9\alpha m_q}$	$\frac{i}{\sqrt{2}}$
$N(^2S_s)\,\frac{1}{2}$	0	$-\frac{k^3}{3\sqrt{6}\alpha^2 m_q}$	$-\frac{1}{6\sqrt{3}}$
$\Delta(^4S_s)\,\frac{3}{2}$	$\frac{k^3}{9\alpha^2 m_q}$	$\frac{k^3}{9\sqrt{3}\alpha^2 m_q}$	$-\frac{1}{4\sqrt{3}}$
$N(^2S_M)\,\frac{1}{2}$	0	$\frac{k^3}{6\sqrt{3}\alpha^2 m_q}$	$\frac{1}{6\sqrt{6}}$
$\Delta(^2S_M)\,\frac{1}{2}$	0	$\frac{k^3}{18\sqrt{3}\alpha^2 m_q}$	$-\frac{1}{3\sqrt{6}}$
$\Delta(^4S_s)\,\frac{3}{2}$	$\frac{k^3}{9\alpha^2 m_q}$	$\frac{k^3}{9\sqrt{3}\alpha^2 m_q}$	$-\frac{1}{4\sqrt{3}}$
$N(^2D_s)\,\frac{5}{2}$	$\frac{2\sqrt{\frac{2}{5}}k^2}{3\alpha^2}$	$-\frac{k^2(k-2m_q)}{3\sqrt{5}\alpha^2 m_q}$	$-\frac{1}{3\sqrt{30}}$
$N(^2D_s)\,\frac{3}{2}$	$-\frac{\sqrt{\frac{2}{5}}k^2}{3\alpha^2}$	$\frac{\sqrt{\frac{2}{15}}k^2(k+3m_q)}{3\alpha^2 m_q}$	$-\frac{\sqrt{\frac{5}{6}}}{6}$
$\Delta(^4D_s)\,\frac{7}{2}$	$\frac{2k^3}{9\sqrt{7}\alpha^2 m_q}$	$\frac{2k^3}{3\sqrt{105}\alpha^2 m_q}-\frac{\sqrt{\frac{3}{70}}}{2}$	
$\Delta(^4D_s)\,\frac{5}{2}$	$-\frac{2k^3}{3\sqrt{35}\alpha^2 m_q}$	$-\frac{\sqrt{\frac{2}{35}}k^3}{9\alpha^2 m_q}$	$-\frac{1}{2\sqrt{105}}$
$\Delta(^4D_s)\,\frac{3}{2}$	$\frac{\sqrt{\frac{2}{5}}k^3}{9\alpha^2 m_q}$	$-\frac{\sqrt{\frac{2}{15}}k^3}{9\alpha^2 m_q}$	$\frac{\sqrt{\frac{5}{6}}}{4}$
$\Delta(^4D_s)\,\frac{1}{2}$	0	$\frac{\sqrt{\frac{2}{15}}k^3}{9\alpha^2 m_q}$	$\frac{\sqrt{\frac{5}{3}}}{4}$
$N(^2D_M)\,\frac{5}{2}$	$-\frac{2k^2}{3\sqrt{5}\alpha^2}$	$\frac{k^2(k-2m_q)}{3\sqrt{10}\alpha^2 m_q}$	$\frac{1}{6\sqrt{15}}$
$N(^2D_M)\,\frac{3}{2}$	$\frac{k^2}{3\sqrt{5}\alpha^2}$	$-\frac{k^2(k+3m_q)}{3\sqrt{15}\alpha^2 m_q}$	$\frac{\sqrt{\frac{5}{3}}}{12}$
$\Delta(^2D_M)\,\frac{5}{2}$	$\frac{2k^2}{3\sqrt{5}\alpha^2}$	$\frac{k^2(k+6m_q)}{9\sqrt{10}\alpha^2 m_q}$	$-\frac{1}{3\sqrt{15}}$
$\Delta(^2D_M)\,\frac{3}{2}$	$-\frac{k^2}{3\sqrt{5}\alpha^2}$	$-\frac{k^2(k-9m_q)}{9\sqrt{15}\alpha^2 m_q}$	$-\frac{\sqrt{\frac{5}{3}}}{6}$

2.4 Configuration Mixing

The amplitudes in the previous subsections are derived under the $SU(6)\otimes O(3)$ symmetry. However, for physical states that symmetry is broken. An example is the violation of the Moorhouse rule [48]. In Ref. [49], a set of parameters C_{N^*} were hence introduced to take into account the breaking of that symmetry, *via* following substitution:

$$O_{N^*} \to C_{N^*} O_{N^*}. \tag{21}$$

In Refs. [49,3], those parameters were allowed to vary around their $SU(6)\otimes O(3)$ values ($|C_{N^*}| = 0$ or 1). In Ref [40], instead of using those adjustable parameters, we introduce the breakdown of that symmetry through the configuration mixings of baryons wave functions.

To achieve such an improvement, we must choose a potential model. The popular used ones are one-gluon-exchange (OGE) model [1,50,51] and Goldstone boson exchange model [52]. As shown in Refs. [5], these two models give similar mixing angles for the negative parity resonances and the relevant observables. An explicit comparison of different potential models in Ref. [53]. In this report

we adopt the OGE model where the Hamiltonian of system can be written as [1,50,51],

$$H = \sum_{i=1}^{3} m_i + \sum_{i=1}^{3} \frac{p_i^2}{2m_i^2} + \sum_{i<j=1}^{3} \tfrac{1}{2} K r_{ij}^2 + \sum_{i<j=1}^{3} U(r_{ij}) + H_{hyp} \,, \tag{22}$$

where the m_i is the "constituent" effective masse of quark i and $\boldsymbol{r_{ij}} = \boldsymbol{r_i} - \boldsymbol{r_j}$ the separation between two quarks. The confinement potential has two components; one written as a harmonic oscillator potential ($\frac{1}{2}Kr_{ij}^2$, with K the spring constant), and an unspecified anharmonicity $U(r_{ij})$, treated as a perturbation.

The hyperfine part interaction is the sum of contact and tensor terms,

$$H_{hyp} = \frac{2\alpha_s}{3m_q^2} \sum_{i<j=1}^{3} \Big\{ \frac{8\pi}{3} \mathbf{S}_i \cdot \mathbf{S}_j \;\; \delta^3(\mathbf{r}_{ij}) + \frac{1}{\boldsymbol{r}_{ij}^3} \big(\frac{3\mathbf{S}_i \cdot \mathbf{r}_{ij}\, \mathbf{S}_j \cdot \boldsymbol{r}_{ij}}{\mathbf{r}_{ij}^2} - \mathbf{S}_i \cdot \mathbf{S}_j \big) \Big\}. \tag{23}$$

Here, $\mathbf{S}_i$ is the spin of quark i, and α_s a normalization factor, treated as free parameter [50].

2.5 Regge trajectories for t-channel

In the literatures, the Regge trajectories have been applied to the study of the pseudoscalar mesons: π [54,55], η [35] and kaon [54,56,57] photoproduction reactions to the describe the higher energy data and well compared with the experiment data. Besides, the results of the MAID Group [35] suggested that It is better to adopt a Reggeized model compared with the t-channel exchanges described by the ρ and ω poles. So, in this work we adopt the Reggeized model to complement our χCQM formalism [38, 40] and study the η production, especially the very recent data released by CBELSA/TAPS [23] and CLAS [24] Collaborations.

In the Reggeized model the main change is substituting the meson exchange poles by the Regge propagator:

$$\frac{1}{t - m_V^2} \to \mathcal{P}^V_{Regge} = \left(\frac{s}{s_0}\right)^{\alpha_V(t)-1} \frac{\pi\alpha'_V}{\sin\left[\pi\alpha_V(t)\right]} \frac{\mathcal{S}_V + e^{-i\pi\alpha_V(t)}}{2} \frac{1}{\Gamma\left(\alpha_V(t)\right)}, \tag{24}$$

where s_0=1 GeV^2 is the reference mass scale and $\mathcal{S}_V = \pm 1$ is the trajectory's signature. The gamma function $\Gamma(\alpha_V(t))$ suppresses poles of the propagator in the unphysical region. The vector-meson Regge trajectory is taken in the following linear form

$$\alpha_V(t) = \alpha_V^\circ + \alpha'_V t, \tag{25}$$

with t the Mandelstam variable, and read for ρ and ω, respectively, as

$$\alpha_\rho(t) = 0.55 + 0.8t, \tag{26}$$
$$\alpha_\omega(t) = 0.44 + 0.9t. \tag{27}$$

3 Results and discussion

With the formalism we developed above, in this report we will study the nucleon resonance spectrum and the η productions with the CM energy up 2.8 GeV.

Table 3. The data sets for the η productions induced by photon and π used in the fitting

Observable	Collaboration/author	W (GeV)	N_{dp}
$\frac{d\sigma}{d\Omega}$ $(\gamma p \to \eta p)$	MAMI94[58]	1.49 - 1.54	100
	CLAS02 [18]	1.53 - 2.12	190
	CLAS09 [24]	1.68 - 2.80	1081
	ELSA05 [19]	1.53 - 2.51	631
	ELSA09 [23]	1.59 - 2.37	680
	LNS06 [20]	1.49 - 1.74	180
	GRAAL07 [21]	1.49 - 1.91	487
Σ $(\gamma p \to \eta p)$	ELSA07 [22]	1.57 - 1.84	34
	GRAAL07 [21]	1.50 - 1.91	150
$\frac{d\sigma}{d\Omega}$ $(\pi^- p \to \eta n)$	Prakhov *et al.* (2005) [17]	1.49 - 1.52	84
	Deinet *et al.* (1969) [11]	1.51 - 1.70	80
	Richards *et al.*(1970) [12]	1.51 - 1.90	64
	Debenham *et al.*(1975) [13]	1.49 - 1.67	24
	Brown *et al.* (1979) [14]	1.51 - 2.45	102

Table 4. Adjustable parameters with their extracted values, where m_q, α_{ho}, Ω, Δ, M, and Γ are in MeV.

	m_q	310 ± 5	α_{ho}	309 ± 2
	α_s	1.60 ± 0.02	Ω	421 ± 4
	Δ	460 ± 1	$g_{\eta NN}$	0.276 ± 0.005
$P_{13}(1720)$	C^γ	0.22 ± 0.01	C^π	-0.85 ± 0.03
New S_{11}	M^γ	1700 ± 1	Γ^γ	473 ± 10
	$C^\gamma_{N^*}$	1.18 ± 0.03		
$N(1535)$	M^γ	1532 ± 1	Γ^γ	140 ± 1
u-channel	C^γ_u	0.71 ± 0.03	C^π_u	1.39 ± 0.05
t-channel	$g_{\rho qq}$	1.90 ± 0.22	$\kappa_{\rho qq}$	-0.20 ± 0.01
	$g_{\omega qq}$	4.88 ± 0.16	$\kappa_{\omega qq}$	-0.26 ± 0.02

3.1 Fitting procedure

Using the CERN MINUIT code, we have fitted simultaneously the following data sets as listed in Table 3. In summary, 3887 experimental values are fitted. Besides, the spectrum is also fitted to the suggested values of Particle Data Group. To do so, we have a total of 19 free parameters, not all of them adjusted on all the data sets, as explained below. In Table 4 we summarize the list of adjustable parameters and their extracted values. Note that the reported uncertainties are those produced by the MINUIT code and should be considered as lower limits.

Using our extracted values for Vqq vertices couplings (Table 4, last four rows) and lead, for VNN vertices, to results reported in Table 5 and compared with results from three other works. Our values for ρ are smaller than those extracted by the MAID analysis [35] and also coming from Bonn [59] and Nijmegen [60] potentials. Note that results from these latter potentials differ between themselves by 30% to 50%. For ω case our value for $g_{\omega NN}$ comes out larger than the MAID analysis [35], but stands in-between those produced by nucleon-nucleon potentials. The $\kappa_{\omega NN}$ deviates significantly from vanishing values of potentials. Detailed discussion on the VNN couplings values can be found in Refs. [25].

The average χ^2 for all data set listed in the Table 3 and spectrum is about 2.4, which suggest the current approaches can reproduced the experiment data generally. In the following we will present our results of spectrum and the η photoproductions as depicted in Fig. 1.

Table 5. Vector-meson nucleon-nucleon couplings.

Ref.	$g_{\rho NN}$	$\kappa_{\rho NN}$	$g_{\omega NN}$	$\kappa_{\omega NN}$
Present work	1.90	3.0	14.6	-0.25
MAID [35]	2.4	3.7	9.0	0
Bonn potential [59]	3.34	6.1	15.8	0
Nijmegen potential [60]	2.76	4.2	11.1	0.02

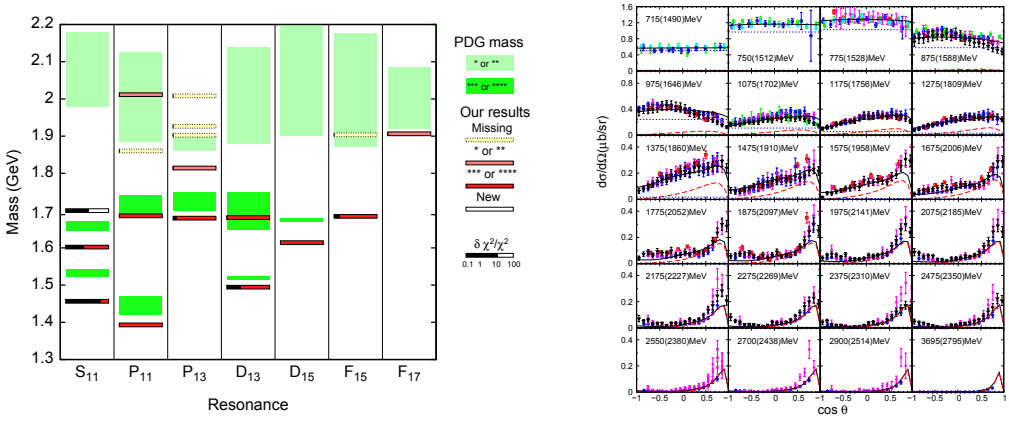

Fig. 1. The spectrum (left) and the differential cross section for η photoproduction (right). The spectrum of baryon resonances from PDG (green bands) and from the present work for known (red bans), missing (yellow bands), and new (white band) resonances. The black bands indicate the variations of χ^2 after turning off the corresponding resonance within our full model. Differential cross section for $\gamma p \to \eta p$ as a function of $cos\theta_\eta$ for various values of photon energy in the lab frame. The values in parenthesis are the corresponding total energy of the system W. The curves are: full model (full), $S_{11}(1535)$ (dotted), and t-channel (Dashed). Data are from Refs. [18–21,23,24, 58].

3.2 Spectrum

Here we present our results for resonances spectrum and roles played by those resonances in the reaction mechanisms of the processes considered in this work.

In Fig. 1 are depicted mass values from PDG isospin 1/2 resonances with $M \lesssim 2$ GeV, our results for the 12 known N^*s, OGE generated missing resonances [38] (P_{11} *(1899)*, P_{13} *(1942)*, P_{13}*(1965)*, P_{13}*(2047)*, and F_{15} *(1943)*) and the introduced third S_{11}. The masses generated by our formalism compare well enough with the PDG values in line with other CQM approaches [50,51]. The same observation is valid for missing resonances, as discussed in our previous work [38]. The new S_{11} has no counterpart within known, neither missing resonances.

In order to investigate the importance of the 18 resonances of our approach, we have switched off each of them one by one. The five missing resonances show no significant effects in line with our previous findings [38]. For the other N^*s, the black part in each bar (Fig. 1) indicates the relative change in χ^2 with that specific resonance turned off. Among the 12 known N^*s, the most significant ones, with decreasing importance, are: $S_{11}(1535)$, $S_{11}(1650)$, $D_{13}(1520)$, $F_{15}(1680)$, $P_{13}(1900)$. Finally, the new $S_{11}(1700)$ appears to be the second most important ingredient of our model.

3.3 Observables for $\gamma p \to \eta p$

In Fig. 1 differential cross section results are depicted at twenty four energies going from close to threshold, E_γ^{lab} =0.715 GeV (W =1.49 GeV) up to E_γ^{lab} =3.70 GeV (W =2.80 GeV). At each en-

ergy three curves are compared with the data: a) full model, b) contribution from solely $S_{11}(1535)$, c) contributions from the Reggeized t-channel. Note that, while full model embodies u-channel, its contribution is too small to be shown in the Figure.

Comparing our model (full curves) with various data shows that the general agreement is acceptable and there is no anomalous behavior in the whole phase space. Discrepancies within those data, in some cases with more than 2σ, make clear problems that have to be faced in fitting such a data base, which is reflected in the χ^2_{dp}=2.5. The dotted curves show contributions due *only* to $S_{11}(1535)$, which has a dominant role near to threshold and up to $W \approx 1.7$ GeV, where t-channel effects already start becoming visible. Note that the dashed curves correspond to contributions *exclusively* from t-channel, without further minimizations. From $W \approx 2$ GeV on, this latter channel gains more and more importance with increasing energy and completely dominates the model results above $W \approx 2.1$ GeV.

In the range $2.2 \lesssim W \lesssim 2.3$ GeV the extreme angles are not very well reproduced, indicating very likely that higher mass N^*s are needed and/or a more extended treatment of the u-channel contributions is desirable. In our work, u-channel contributions turn out to be very small in the whole energy region, with a maximum contribution of roughly 8% around $W \approx 1.65$ GeV and almost vanishing above $W \approx 1.9$ GeV.

4 Summary

In this report we introduce our chiral quark model in the η productions. Starting from the chiral effective Lagrangian, the amplitudes for the meson productions can be derived by the second-quantization method, and connected to the usually helicity amplitudes and decay amplitudes. With this connections the $SU(3)$ symmetry breaking can be introducing through the configuration mixings, which can be calculated from the potential models. For the higher energy region, the Regge trajectories are introduced to describe the new released data by CLAS and CBELSA/TAPS. One advantage of our approaches is that the spectrum and the observables for the meson productions can be investigated in the same time. With such formalism the η productions can be calculated and compared well with the experiment data with few parameters.

References

1. N. Isgur, G. Karl, Phys. Lett. **B72**, 109 (1977)
2. N. Isgur, Phys. Rev. **D62**, 054026 (2000)
3. B. Saghai, Z. Li, Eur. Phy. J. **A11**, 217 (2001)
4. J. Chizma, G. Karl, Phys. Rev. **D68**, 054007 (2003)
5. J. He, Y.-B.Dong, Nucl. Phys. **A725**, 201 (2003)
6. J. He, Y.-B.Dong, J. Phys. **G29**, 2737 (2003)
7. S. Capstick, W. Roberts, Fizika **B13**, 271 (2004)
8. B. Saghai, Z. Li, Few Body Syst. **47**, 105 (2010)
9. C. S.An, B. S.Zou, Eur. Phys. J. **A39**, 195 (2009)
10. C.-S.An, B.-S.Zou, Sci. Sin. **G52**, 1452 (2009)
11. W. Deinet, et al., Nucl. Phys. **B11**, 495 (1969)
12. W. B.Richards, et al., Phys. Rev. D**1**, 10 (1970)
13. N. C.Debenham, et al., Phys. Rev. **D12**, 2545 (1975)
14. R. M.Brown, et al., Nucl. Phys. **B153**, 89 (1979)
15. M. Clajus, B. M. K.Nefkens, PiN Newslett. **7**, 76 (1992)
16. T. W.Morrison, Ph.D. thesis, The George Washington University 1999
17. S. Prakhov, et al., Phys. Rev. **C72**, 015203 (2005)
18. M. B.Dugger, et al. Phys. Rev. Lett. **89**, 222002 (2002)
19. V. Crede, et al., Phys. Rev. Lett. **94**, 012004(2005)
20. T. Nakabayashi, et al., Phys. Rev. **C74**, 035202 (2006)
21. O. Bartalini, et al., Eur. Phys. J. **A33**, 169 (2007)

22. D. Elsner, et al., Eur. Phys. J. **A33**, 147 (2007)
23. V. Crede, et al., Phys. Rev. **C80**, 055202 (2009)
24. M. Williams, et al., Phys. Rev. **C80**, 045213 (2009)
25. G. Penner, Ph.D. thesis, Universität Giessen (2002)
26. A. V.Anisovich, et al., Eur. Phys. J. **A25**, 427 (2005)
27. S. Ceci, A. Svarc and B. Zauner, Phys. Rev. Lett. **97**, 062002 (2006)
28. R. A.Arndt, W. J.Briscoe, I. I.Strakovsky and R. L. Workman, Int. J. Mod. Phys. **A22**, 349 (2007)
29. T. P.Vrana, S. A.Dytman and T. S. H. Lee, Phys. Rept. **328**, 181 (2000)
30. A. Matsuyama, T. Sato and T. S. H.Lee, Phys. Rept. **439**, 193 (2007)
31. G.-Y.Chen, S. Kamalov, S. N.Yang, D. Drechsel and L. Tiator, Nucl. Phys. **A723**, 44 (2003)
32. A. Gasparyan, J. Haidenbauer, C. Hanhart and J. Speth, Phys. Rev **C68**, 045207 (2003)
33. B. Julia-Diaz, B. Saghai, T.-S.Lee and F. Tabakin, Phys.Rev. **C73**, 055204 (2006)
34. J. Durand, B. Julia-Diaz, T. S. H.Lee, B. Saghai and T. Sato, Phys. Rev. **C78**, 025204 (2008)
35. W.-T.Chiang, B. Saghai, F. Tabakin, and T. S. H.Lee, Phys. Rev. **C69**, 065208 (2004).
36. Q. Zhao, J. S.Al-Khalili, Z. P.Li and R. L.Workman, Phys. Rev. **C65**, 065204 (2002)
37. J. He, B. Saghai, Z. Li, Q. Zhao and J. Durand, Eur. Phys. J. **A35**, 321 (2008)
38. J. He, B. Saghai and Z. Li, Phys. Rev. **C78**, 035204 (2008)
39. X.-H.Zhong, Q. Zhao, J. He and B. Saghai, Phys. Rev. **C76**, 065205 (2007)
40. J. He, B. Saghai, Phys. Rev. **C80**, 015207 (2009)
41. A. Manohar, H. Georgi, Nucl. Phys. **B234**, 189 (1984)
42. Z.-p.Li, H.-x.Ye and M.-h.Lu, Phys. Rev. **C56**, 1099 (1997)
43. M. Jacob and G. C. Wick, Annals Phys. **7** 404 (1959)
44. R. L. Walker, Phys. Rev. **182** 1729 (1969)
45. A. Hosaka, M. Takayama and H. Toki, Nucl. Phys. A **678** 147 (2000)
46. G. Karl and E. Obryk, Nucl. Phys. B **8** 609 (1968)
47. V. Chaloupka *et al.* [Particle Data Group], Phys. Lett. B **50** 1 (1974)
48. R. G. Moorhouse, Phys. Rev. Lett. **16** 772 (1966)
49. Z.-p.Li, B. Saghai, Nucl. Phys. **A644**, 345 (1998)
50. N. Isgur, G. Karl, Phys. Rev. **D18**, 4187 (1978)
51. N. Isgur, G. Karl, Phys. Rev. **D19**, 2653 (1979)
52. L. Y. Glozman and D. O. Riska, Phys. Rept. **268**263 (1996)
53. J. He, S. G. Yuan and H. S. Xu, arXiv:1105.1600 [nucl-th]
54. M. Guidal, J. M.Laget and M. Vanderhaeghen, Nucl. Phys. **A627**, 645 (1997)
55. A. Sibirtsev, et al., Eur. Phys. J. **A34**, 49 (2007)
56. T. Corthals, J. Ryckebusch and T. Van Cauteren, Phys. Rev. **C73**, 045207 (2006)
57. P. Vancraeyveld, L. De Cruz, J. Ryckebusch and T. Van Cauteren, Phys. Lett. **B681**,428 (2009)
58. B. Krusche, et al., Phys. Rev. Lett. **74**, 3736 (1995)
59. R. Machleidt, K. Holinde and C. Elster, Phys. Rept. **149**, 1 (1987)
60. T. A.Rijken, Phys. Rev. **C73**, 044007 (2006)